Clay Swelling in Dry Supercritical Carbon Dioxide: Effects of Interlayer Cations on the Structure, Dynamics, and Energetics of CO_2 Intercalation Probed by XRD, NMR and GCMD Simulations

Narasimhan Loganathan[1,] Geoffrey M. Bowers[2], A. Ozgur Yazaydin[1,3] H. Todd Schaef[4], John S. Loring[4], Andrey G. Kalinichev[5] and R. James Kirkpatrick[6]*

[1] Department of Chemistry, Michigan State University, East Lansing, Michigan 48824, United States

[2] Department of Chemistry and Biochemistry, St. Mary's College of Maryland, St. Mary's City, Maryland 20686, United States

[3] Department of Chemical Engineering, University College London, London, WC1E7JE, United Kingdom

[4] Pacific Northwest National Laboratory, Richland, WA, 99352, United States

[5] Laboratoire SUBATECH (UMR 6457 - Institut Mines-Télécom Atlantique, Université de Nantes, CNRS/IN2P3), 44307, Nantes, France

[6] College of Natural Science, Michigan State University, East Lansing, Michigan 48824, United States

[*] **Corresponding author e-mail:** naresh20@msu.edu

Telephone: (+1)517-353-1106

Abstract

I*n situ* XRD and NMR experiments combined with molecular dynamics simulations using the grand canonical ensemble (GCMD) show that cation size, charge and solvation energy play critical roles in determining the interlayer expansion of smectite clay minerals when exposed to dry *sc*CO_2 under conditions relevant to petroleum reservoirs and geological CO_2 sequestration conditions. The GCMD results show that the smectite mineral, hectorite, containing interlayer alkali and alkaline earth cations with small ionic radii and high solvation energies (e.g., Na^+ and Ca^{2+}) does not intercalate CO_2 and that the fully collapsed interlayer structure is the energetically most stable configuration. With Cs^+ and Ba^{2+} the monolayer structure is the stable configuration, and CO_2 should spontaneously enter the interlayer. With Cs^+ there is not even an energy barrier for CO_2 intercalation, in agreement with the XRD and NMR results. ^{13}C NMR and simulations show that the average orientation of the intercalated CO_2 is with their O-C-O axes parallel to the basal clay surface and that undergo a rapid rotation about an axis perpendicular to the main molecular axis. The simulations show that the strength of the interaction between the exchangeable cation and the clay structure dominates the intercalation energetics in dry scCO_2.

Introduction

Injection of CO_2 into deep geological formations and depleted oil and gas reservoirs is an effective method for enhancing oil recovery and a potential pathway for reducing anthropogenic CO_2 in the atmosphere. Target geological storage sites are primarily composed of porous rock formations in which the CO_2 is confined by overlying caprocks that act as low permeability barriers to upward fluid flow.[1-8] Long-term confinement of CO_2 depends strongly on its interactions with these caprocks, which are typically shales containing significant amounts of clay minerals. Intercalation and nano-confinement of fluids in the 2-dimensional interlayer galleries of expandable clays (principally smectites and smectite layers in mixed layer illite-smectites) may affect the properties and porosity of the caprocks by expanding or shrinking the interlayer pores (tracked via the basal spacings)[9-24] and can lead to substantial changes in the structural and dynamical behavior of the intercalated fluid molecules with respect to the bulk fluid phase. Numerous studies[25-39] provide critical molecular-scale information about the role of the clay composition, location of its structural charge, and the properties of the charge compensating cation in determining the structure, dynamics, energetics and reactivity of H_2O in the interlayer galleries and inter-particle pore space.

Recent experimental and molecular simulation studies at conditions relevant to subsurface injection of supercritical CO_2[9-23,40-48] have shown that the intercalation and retention of CO_2 in smectite interlayers is possible but depends strongly on the amount and thermodynamic properties of water in the system. For example, Giesting et al.[11,12] and Schaef et al.[17,19] have shown that the H_2O saturation state (relative humidity, R.H.) of supercritical CO_2 ($scCO_2$) controls CO_2 intercalation in Na-, Mg- and Ca-montmorillonite at 323 K and 90 bar. The results show that no CO_2 enters the dry and collapsed interlayers of these smectites and that CO_2 intercalation only occurs in the presence of at least a sub-monolayer of H_2O. This humidity-dependent intercalation was further validated by Loring et al.,[20-22] who also showed

that the maximum CO_2 intercalation at 90 bar and 323 K occurs when the interlayer H_2O content is equivalent to that of a monolayer hydrate structure. *In situ* experimental NMR, IR, and XRD of the similar smectite mineral, hectorite, at 90 bar CO_2 and 323 K by Bowers et al.[9] showed that the properties of the charge balancing cation can greatly change the CO_2 intercalation behavior. These results show that for the cations with relatively high hydration energies and small ionic radii (Na^+, Ca^{2+}), CO_2 intercalation requires the presence of H_2O molecules to prop open the interlayers. In contrast, Cs^+ with a larger ionic radius and smaller hydration energy allows Cs-hectorite to intercalate CO_2 readily even in the complete absence of water (R.H. of the $scCO_2 = 0$). With all three cations, increasing H_2O saturation of the $scCO_2$-rich fluid phase causes a decreasing interlayer molar $CO_2/(CO_2+H_2O)$ ratio, with Cs-hectorite maintaining a higher ratio at all conditions. Computational molecular simulations of nano-confined CO_2-H_2O mixtures in smectites in equilibrium with water-saturated CO_2 at 348 K and 125 bar using the grand canonical Monte Carlo (GCMC) ensemble by Botan et al.[40] have suggested that the stable state of Na-montmorillonite exposed to supercritical CO_2 is the bilayer hydrate (basal spacing ~15.0 Å) but that maximum CO_2 intercalation occurs at the monolayer hydrate state. Recently GCMC simulations by Kadoura et al.[41] show that for montmorillonite at high R.H.s ($\geq$ 60%) at 323 K and 90 bar there is no significant difference in the interlayer CO_2 content with cations having different hydration energies (Na^+, Ca^{2+}, Mg^{2+}). Simulation studies using GCMC and Gibbs ensemble Monte Carlo (GEMC) have indicated that for Na-smectite under similar conditions CO_2 intercalation can vary depending on the clay layer charge and its structural location.[42-45] Recently, we reported grand canonical molecular dynamics (GCMD) simulations that show that varying temperature (323–368 K) and pressure (90-150 bar) have little impact on the structural environments and dynamics of intercalated CO_2 molecules in Na-hectorite in equilibrium with H_2O-saturated $scCO_2$.[48]

Intercalation of dry CO_2 in smectite interlayers has been less extensively studied but is important as a limiting energetic and structural case and may have significant application to situations when dry CO_2 is injected into the subsurface. Mineralogical studies using X-ray computed tomography before and after CO_2 injection have suggested that $scCO_2$ can laterally displace the brine in that occupies the pore volumes of the host sedimentary rocks causing either anhydrous or nearly anhydrous conditions, especially during the early stages of injection.[1,6,49,50] Under these circumstances, the dry CO_2 could potentially enter and dehydrate the smectite interlayers, cause swelling or shrinking of the clay, and thus generate mechanical stresses and alter the overall pore structure of shale caprocks. It could also suppress hydration reactions involving the mineral phases due to a lack of residual H_2O in the pore fluid. Our previous experimental studies have shown that collapsed Na-montmorillonite does not intercalate CO_2 or expand when exposed to dry CO_2 under reservoir conditions (323 K and 90 bar), whereas Cs- and NH_4-montmorillonite do.[51] Parallel GCMD calculations are consistent with these results, showing a large energy barrier for CO_2 intercalation in Na-montmorillonite but no such barrier Cs- and NH_4-montmorillonites.[51] These results suggest that the exchangeable cation has a significant effect on the intercalation behavior under dry CO_2 conditions, although the energetic origin of these effects and the associated structural and dynamical behavior have not been explored in detail.

In the present work, we combine *in situ* experimental nuclear magnetic resonance spectroscopy (NMR) and X-ray diffraction (XRD) studies at a CO_2 pressure of 90 bar and a temperature of 323K with GCMD calculations to investigate the structure, dynamics and energetics of the intercalation of dry CO_2 in the smectite mineral, hectorite, containing monovalent and divalent cations spanning a range of hydration and solvation properties. We used hectorite as our host material for the experiments and modeling studies, because it has a very low Fe content that improves NMR spectral resolution by minimizing paramagnetic

effects affecting most natural montmorillonites. Like montmorillonite, hectorite develops most of its permanent structural charge by cation substitution in the octahedral layer, and it has been used for many NMR studies to examine smectite behavior.[9,24,26,28,29,31,52]

Experimental Methods

In Situ XRD

Na- and Cs-exchanged hectorite samples were characterized by XRD at 323 K first under vacuum (10^{-3} Torr) and then during exposure to dry CO_2 at a pressure of 90 bar using high pressure and temperature X-ray diffraction techniques previously described.[9,17,19,51] The Cs-hectorite was also reexamined under vacuum conditions at 323K after the CO_2 was removed. The base hectorite was SHCa-1, which is available at the Clay Source Repository of the Clay Minerals Society.

Hectorite is a 2:1 trioctahedral smectite clay mineral that develops negative structural charge due to Li^+ for Mg^{2+} substitution in the octahedral layer. The structural formula of this sample, that was processed to remove carbonate and quartz impurities, is $[M_{0.36}(Mg_{2.65}Li_{0.35})(Si_{3.99}Al_{0.01})O_{10}(F_{1.1}OH_{0.9})]$.[28,29] For these experiments, measured aliquots of dilute clay suspensions in water were pipetted onto a beryllium post, with each sample occupying a circular area with an approximate diameter of 2-3 mm. Each clay sample was allowed to air dry to produce a thin preferentially oriented film. The beryllium post was then placed on an *XYZ* stage and the samples were aligned with the aid of a laser system, allowing exposure of only one clay film at a time to the XRD beam. Once the sample coordinates were established, the pressurized reactor was assembled, mounted into the instrument, and heated to 323 K. Subsequent exposure to vacuum for 30 minutes removed most of the water from the clay samples. Pressurization with CO_2 was accomplished through an ISCO pump connected directly to the reactor.

XRD patterns were collected using a Bruker D8 Discover instrument with a rotating Cu anode (CuK alpha = 1.5418 Å), a programmable *XYZ* customized stage, and a Vantec 500 detector set at a sample-to-detector distance of 15 cm. This instrument, operated at 50 kV and 24 mA, is capable of producing an intensely focused 0.5 mm beam. XRD patterns for each sample were acquired for 300 seconds, integrated over a 2ϑ range of 4-45°, and subsequently analyzed with the MDI JADE® XRD software package to obtain peak positions and peak profiles.

In Situ MAS NMR

In situ ^{13}C MAS NMR spectra were obtained at 323 K and 90 bars P_{CO2} for the same Na- and Cs-exchanged hectorite samples examined by XRD using the high pressure apparatus that has been described previously.[9,24] For these experiments, clay filled rotors were dried overnight in a vacuum oven at 323K and 10^{-3} Torr. The rotors were sealed after backfilling the vacuum oven with dry N_2 gas. Hectorite samples prepared in a similar way and analyzed by IR spectroscopy show no detectable H_2O content with Cs^+ and ≤ 0.5 H_2O per cation with Na^+. 99% isotopically enriched $^{13}CO_2$ was then introduced into the rotor using a one-way flow system.[53,54] The spectra were collected using a 7.0 T Varian DDR 2 console with a 5 mm HXY probe at a spin frequency of 3 kHz using a $\pi/2$ pulse width of 5 μs, a spectral width of 50 kHz, and a 30 s inter-pulse delay to obtain 3000 transients. The ^{13}C spectra were referenced to tetramethylsilane (TMS) through a secondary standard of adamantane using the high-frequency peak. All NMR data were processed using iNMR, a commercial program by MestReC, and all NMR results were iteratively fit using Abscissa, a freeware app written by Rudiger Bruhl. For ^{13}C, the first two data points were removed due to acoustic ringing before zero filling to 32k points and applying 20 Hz of exponential apodization. In almost all cases a standard baseline correction was performed to flatten the baseline. All peak fits were performed by iteratively fitting the data set to Lorentzian lineshapes.

Simulation Methods

The model hectorite used in our simulations has a structural formula of $M^{+}(Mg_5Li)Si_8O_{20}(OH)_4$. This model has no tetrahedral substitutions, in accordance with the experimental sample, which contains a negligible fraction (0.25%) of tetrahedral Al^{3+} for Si^{4+} substitution.[9,26,28,29,31] The simulation model, however, differs from the experimental sample in two important respects. First, the model has a 30% higher layer charge. Second, the OH^- site in the model contains only OH^- groups, whereas the experimental sample has 55% F^- for OH^- substitution. The hydration behavior of synthetic fluoro-hectorite has been discussed previously.[27,55,56] Previous simulation studies employing this model have shown good agreement with experimental data justifying its use here.[30,33,35,47,48]

The simulation supercell consists of 16 crystallographic unit cells of hectorite (4 × 2 × 2) encompassing two interlayer galleries with surface areas of 360.23 $Å^2$. This supercell size is sufficient to eliminate any finite size effects. Isomorphic substitutions of Li^+/Mg^{2+} in the supercell were performed in a quasi-disordered pattern following Lowenstein's rule to prevent Li^+-O-Li^+ next nearest neighbor arrangements.[57] The structural details of the model are described elsewhere.[30,33,35,48] Overall charge balance for the model is obtained by cation substitution in the interlayer galleries. Nine different compositions were simulated, each with the interlayer occupied by a single type of alkali or alkaline earth cation (Li^+, Na^+, K^+, Rb^+, Cs^+, Mg^{2+}, Ca^{2+}, Sr^{2+}, or Ba^{2+}).

Molecular dynamics simulations were performed in the grand canonical ensemble using the RASPA software package.[58,59] Basal spacings were varied from 9.0 Å to 18.0 Å at steps of 0.2 Å and were constrained at the initial value throughout each simulation run. All of the charge compensating cations were initially placed randomly in the interlayer region and were allowed to move during the GCMD runs. Importantly, during the simulations we permit lateral movements of the T-O-T layers parallel to each other (in the *x* and *y* directions) without

disrupting the structure. These translational movements are essential, because the minimum energy interlayer structure depends on the relative positions of the adjacent T-O-T layers and varies with the type of the interlayer cation and the number of intercalated fluid molecules, as reported in previous studies.[40,48,51,60]

All the GCMD simulations were performed as described in our previous study of H_2O and CO_2 exchange in Na-hectorite.[48] The GCMD approach is a hybrid technique which incorporates both Monte Carlo and molecular dynamics procedures by sampling the insertion and deletion of fluid molecules with equal probability at every MD time step. Therefore, temperature, volume and the chemical potential (μ) of the fluid molecules are fixed in our simulations, but the number of fluid molecules absorbed in the interlayer can fluctuate. The interatomic interactions for the T-O-T clay structure and the metal cations were described using the ClayFF force field,[61] which is widely used in clay interfacial simulations. The CO_2 molecules were represented using the rigid EPM2 model.[62] Three-dimensional periodic boundary conditions were employed with a cutoff of 9.0 Å for short range non-electrostatic interactions, and the long-range electrostatic interactions were computed using Ewald summation[63] with an accuracy of 10^{-6}. Fugacities are required to determine the acceptance of insertion and deletion moves for the fluid species (here CO_2) and were calculated using the Peng-Robinson equation of state.[64]

All simulations were performed at T=323 K and P=90 bar (the experimental conditions described above) for 15 ns to reach equilibrium followed by another 10 ns of data production with a time step of 1 fs. The reported adsorption profile and related energetics, interlayer structure and dynamics were calculated using the data from the last 5 ns of each equilibrium simulation run. The methods of analysis can be found in our previous papers.[33,35,48,65] The computed energetics of each system is evaluated using the immersion energies, which were computed by considering the largest basal spacings (18.0 Å) as the reference state because its

value is the closest to that of bulk CO_2 than any other basal spacing. The use of immersion energies to investigate the equilibrium states of smectites have been discussed previously mostly for water adsorption[33,35,37,48,51,65] and is extended here to CO_2.

Results and Discussion

XRD

The *in situ* XRD results (Figure 1) show that the basal spacing (d_{001} basal reflection) of Cs-hectorite increases reversibly by about 1 Å on exposure to dry CO_2, but that the basal spacing of Na-hectorite does not change. We interpret these results to indicate that under our experimental conditions, CO_2 readily enters the interlayer galleries of Cs-hectorite but not Na-hectorite. The specific basal spacings of the Cs-hectorite before and after exposure to dry CO_2 (11.06 Å and 12.05 Å, respectively) are the same as previously reported.[9] They are also consistent with values reported in the literature for similar samples and conditions.[33,37,51,57,65,66] After a few minutes of exposure to vacuum conditions following equilibration with dry $scCO_2$, the basal spacing of Cs-hectorite returns to its original value, suggesting that there is not a significant quantity of recalcitrant CO_2 in the interlayers.[9] For Na-hectorite, previous *in situ* IR data for this sample[9] show nearly complete removal of interlayer water and a lack of expansion when exposed to dry $scCO_2$. Fully dehydrated Na-SHCa-1 sample has a basal spacing of 9.7 Å,[26] and the value of 9.81Å observed here indicates removal of all or most of the interlayer water. In addition, XRD did not detect formation of a carbonate phase in either the Cs- or Na-hectorite.

^{13}C MAS NMR

As for the XRD results, the ^{13}C MAS NMR results indicate sorption of CO_2 in the interlayers of Cs-hectorite but not Na-hectorite. As discussed by Bowers, et al.,[9] the spectrum of CO_2 in an empty rotor and with Na-SHCa-1 are very similar (Figure 2). Both contain a center band at ~124 ppm with a full width at half height (FWHH) of ~0.11 ppm that represents CO_2 molecules that are undergoing rapid, isotropic tumbling in the supercritical fluid phase and that

experience little interaction with the clay surface.[9] Both these samples also show a pair of small spinning sidebands (SSBs). For the scCO_2 without clay present, these SSBs must be associated with CO_2 either adsorbed on the rotor wall or being compressed and densified against the wall due to the centrifugal forces caused by the rotor rotation. For the Na-SHCa-1 sample, the SSBs are likely to arise from similar effects, possibly including weak adsorption on or compressed against the exterior surfaces of the clay particles.[9] Note that the spectrum for the Na-SHCa-1 sample in Figure 2 is greatly expanded vertically to show the SSBs. In contrast, for the Cs-hectorite, the center band is much broader, with a FWHH of 0.67 ppm, and there is a broader, asymmetric spinning sideband manifold. The sideband manifold for this sample is very similar to that reported previously for Cs-hectorite dried over P_2O_5 or equilibrated at 43% R.H. before exposure to dry *sc*CO_2.[9] It indicates a residual chemical shift anisotropy (CSA) associated with adsorption of CO_2 molecules in an environment where they undergo anisotropic rotation. We previously assigned this pattern to adsorbed CO_2 molecules in a monolayer hydrate-type (~12.5 Å) interlayer arrangement with their long (O=C=O) molecular axes having a time-averaged orientation parallel to the basal clay surface and experiencing rapid (>10^5 Hz) reorientation about an axis normal to the clay basal surface.[9]

The ^{13}C MAS NMR spectra for Cs-hectorite here are also similar to those published previously for Cs-exchanged Wyoming montmorillonite (Cs-SWy-2) with dry CO_2 at 90 bar and 323 K.[51] Most importantly, both show similar SSB patterns indicating CO_2 intercalation into the interlayer galleries where confinement induces restricted molecular reorientation. For the Cs-hectorite, however, the sidebands have on average a FWHH of ~2.92 ppm, compared to ~1.37 ppm for the Cs-montmorillonite. The FWHH of the center band for the Cs-hectorite is also about twice that of the center band of the Cs-montmorillonite. This difference is surprising, because SWy-2 contains substantially more structural Fe than SHCa-1,[9,29,31,51] and we expected that its ^{13}C NMR spectrum would show significant paramagnetic broadening as a

result. Thus, it appears that in Cs-montmorillonite the motion of the CO_2 molecules is effectively decoupling the ^{13}C and electron spin systems. The origin of the differences in peak widths for the Cs-hectorite and montmorillonite are uncertain at this time, but may be due to dynamical disorder, small differences in the interlayer *z* dimension, or differences in the NMR powder averaging behavior related to the mean particle size, crystallite size, and packing density/geometry in the rotors. The spectrum for Cs-hectorite was obtained with a 5 mm rotor, whereas that for the Cs-montmorillonite was obtained with a 7.5 mm rotor, and the Cs-hectorite samples are ground and sieved to provide a controlled particle size in the rotors. In general, the *sc*CO_2 fluid pockets in the center of the rotor cavity are larger with 7.5 mm than with 5 mm rotors, which may influence the exchange of CO_2 between interlayer and bulk fluid environments.

Computational Results

Adsorption Profile and Energetics

The computational modeling results show that the properties of the exchangeable cations have significant effects on the structural and energetic behavior of smectite-CO_2 systems and are in good agreement with the experimental results discussed above. For all the simulated systems, CO_2 intercalation begins at a basal spacing of ~11.0 Å except with Mg^{2+}, for which it begins at ~10.7 Å. The amount of intercalated CO_2 then increases stepwise with increasing basal spacing (Figures 3a and 3b). Except with Cs^+, the basal spacing at which intercalation begins is greater than the basal spacings of the fully collapsed structures.

In parallel, the computed immersion energies show an energy barrier to CO_2 intercalation that decreases with increasing cation size for both the alkali and alkaline earth series (Figures 3c and 3d). This energy barrier is the difference between the maximum energy of the system (typically near 10.5 – 11.0 Å) and the value for the fully collapsed structure with the same cation. With Cs^+, there is no energy barrier, and the immersion energy decreases

continuously from that of the collapsed structure to the first energy minimum near 12.5 Å. With K^+, Rb^+, Sr^{2+}, and Ba^{2+}, the barrier is quite small, but it is much larger with Li^+, Na^+, Mg^{2+} and Ca^{2+}. With Li^+, Na^+, Mg^{2+} and Ca^{2+}, the global minimum energy structure is the collapsed state, whereas it is the monolayer structure near 12.5 Å with K^+, Rb^+, Cs^+, Sr^{2+} and Ba^{2+}.

We interpret these results to show that CO_2 should spontaneously enter the interlayer galleries of fully dehydrated and collapsed K^+, Rb^+, Cs^+, Sr^{2+}, and Ba^{2+} hectorite, but not Li^+, Na^+, Mg^{2+} and Ca^{2+} hectorite. This conclusion is in full agreement with the experimental XRD results above that show CO_2 intercalation in Cs-hectorite but not Na-hectorite. Note that the computed immersion energies here are not free energies and do not include entropic effects. This could make a difference in interpreting relatively small immersion energy differences between the monolayer and bilayer structures of the K^+, Rb^+, Cs^+, Sr^{2+}, and Ba^{2+} systems, but are unlikely to be significant for interpreting the results for the Li^+, Na^+, Mg^{2+} and Ca^{2+} systems. The computed intercalation energies are consistent with the results of comparable GCMD calculations for Na-, NH_4-, and Cs-montmorillonite, which show a large barrier to CO_2 intercalation with Na^+ but essentially no barrier with NH_4^+ and Cs^+.[51] This conclusion is also consistent with the free energy calculations by Makaremi et al.[43], which show a large energy barrier for CO_2 intercalation into Na-montmorillonite.

The relationship between the basal spacings and computed energies that highlight the need to prop open the interlayers of smectites that contain relatively small charge-balancing cations to allow CO_2 intercalation, as observed in previous experimental and simulation studies.[9-14,16-23,40-45,48] These studies have indicated that the small cations with high hydration energies, the interlayers needed to be propped open by some H_2O molecules to incorporate CO_2, and the maximum CO_2 intercalation (maximum CO_2/CO_2+H_2O ratio) occurs near the monolayer hydrate interlayer structure.[9-14,40-45,48] To our knowledge, there have been no studies of CO_2 intercalation in pillared clays, which are propped open by interlayer precipitates.

For all the simulated systems here, the increase in interlayer CO_2 content with increasing basal spacing shows 2 broad plateaus between 12.4-13.5 Å and 15.5-16.3 Å (Figures 3a and 3b), corresponding to monolayer and bilayer CO_2 structures, respectively. In parallel, the immersion energies have broad minima at the same basal spacing ranges (Figures 3c and 3d). Basal spacings associated with monolayer CO_2 adsorption were previously reported for Na-fluorohectorite exposed to gaseous CO_2 at much lower temperature and pressure conditions (253 K and 15 bar) using XRD.[67] For our hectorite simulations with Li^+, Na^+, Mg^{2+} and Ca^{2+}, these monolayer and bilayer structures are metastable with respect to the collapsed structures, and for Na-hectorite interlayer adsorption of CO_2 is not experimentally accessible. We expect fully dry Li-, Mg-, and Ca-hectorites to behave in the same way. As for the Cs-hectorite XRD experiments and simulations, the computational results suggest that dry hectorite exchanged with K^+, Rb^+, Sr^{2+}, and Ba^{2+} should intercalate CO_2 and expand. For the Cs-hectorite simulations reported here, the monolayer structure is the experimentally observed stable state, in agreement with the global energy minimum in the computed immersion energy at the monolayer structure compared to the bilayer structure. This is also the case with Rb^+, K^+, Sr^{2+} and Ba^{2+}. However, with divalent cations, the immersion energy differences between the monolayer and bilayer structures are small.

For our systems with alkali cations, the computed interlayer CO_2 content decreases as the size of the cation increases from Li^+ to Cs^+. For the monolayer structures this decrease is from 2.7 to 1.8 CO_2 per unit cell, and for the bilayer structures, it is from 5.0 to 3.8 molecules per unit cell. In contrast, with the alkaline earth cations cation size has no effect on the amount of intercalated CO_2, with all systems showing ~2.6 and ~5.3 CO_2 per unit cell at the monolayer and bilayer spacings, respectively. The decreasing interlayer CO_2 content with increasing ionic radii with the alkali metal cations correlates well with experimental and simulation studies of montmorillonite exposed to dry CO_2 under identical thermodynamic conditions.[51] In contrast,

recent experimental study by Bowers et al.[9] have reported that the interlayer CO_2 content of Cs-hectorite exposed to $scCO_2$ with increasing water content is greater than that of Na-hectorite. This difference is probably due to the larger hydration energy of Na^+ causing more interlayer H_2O adsorption leaving less open interlayer space for CO_2 intercalation in the studies by Bowers et al.[9] However, under dry $scCO_2$ exposure, the smaller the size of the cation, the larger the interlayer space available for CO_2 intercalation thus leading to higher CO_2 content for Na- than Cs-hectorite.

In the current study, at any given basal spacing, the number of intercalated CO_2 molecules per cation is always greater with the alkaline earth cations than with the alkali cations. As discussed in our previous experimental and simulation studies,[9,19] this difference can be attributed to the smaller number of divalent cations required to compensate the hectorite layer charge, thereby increasing the interlayer space accessible for CO_2 compared to smectites with monovalent cations. With alkali cations the plateau regions also become increasingly flat with increase in ionic size, whereas the plateau shapes are similar for all the alkaline earth cations. This is likely because the change in ion size is substantially greater for the alkali cation series (Li^+ *vs* Cs^+) than the alkaline earth cation series (Mg^{2+} *vs* Ba^{2+}). The absence of substantial differences with the different alkaline earth cations despite the ~160 kJ/mol difference in the CO_2 solvation energies between Mg^{2+} and Ba^{2+} supports the geometrical origin of this effect.

The energetic contributions from the cation-clay layer, cation-CO_2, and CO_2-clay layer interactions provide deeper insight into the origin of the dependence of the CO_2 intercalation on the properties of the cation and demonstrate that the magnitude of the interaction between the cation and the clay T-O-T layers dominates this behavior (Figure 4). For both the alkali and alkaline earth cation series, the magnitude of the cation-clay layer interaction for the fully collapsed structures decreases (becomes less negative) with increasing cation size (Figures 4a

and 4b). The energies at the collapsed basal spacings are the relevant comparators, since for each system expansion starts from this value. With the alkali cations, this energy varies from -3675.3 kJ/mol with Li^+ to -3400.1 kJ/mol with Cs^+, and with the alkaline earth cations it varies -3764.9 kJ/mol with Mg^{2+} to -3487.9 kJ/mol with Ba^{2+}. Importantly, the difference in the clay-cation interaction energies between the collapsed structures and the basal spacings at which intercalation begins (~11.0Å) is large for cations with high hydration energies and decreases with increasing cation size. Hence, there is a cost of >~150 kJ/mol in the clay-cation interaction energies with Li^+, Na^+, Mg^{2+} and Ca^{2+} for any CO_2 to intercalate, in contrast to <~60kJ/mol with the other cations. At monolayer spacings the clay-cation interaction energies are very similar for both the alkali and alkaline earth cations, and the differences at larger basal spacings are very small. Despite a need for only half the number of cations to compensate the layer charge with the alkaline earth cations vs. the alkali cations, the magnitude of the interaction energies for both types of cations with the clay surface are very similar. This similarity indicates that the divalent cations have a greater interaction energy per cation with the clay structure than the monovalent cations, as expected from the charge differences. For the cation-CO_2 interactions at a given basal spacing, the interaction energies are negative and decrease (becomes less negative) with increasing cation size in each cation series. They are larger in general for the alkaline earth series (Figures 4c and 4d). Both these trends are expected based upon recently computed cation-CO_2 solvation energies in $scCO_2$ fluid.[51,68] The interaction energies of CO_2 molecules with the clay structure are slightly negative but do not vary greatly with the different alkaline and alkaline earth cations (Figures 4e and 4f). Together, these results show that the increase in the cation-CO_2 interaction energy with decreasing cation size cannot overcome the decreasing cation-clay interaction energy in the absence of H_2O.

Computed Interlayer Structure

It is normally not possible to determine the detailed arrangement of the cations and fluid molecules in smectite interlayer galleries by diffraction methods due to static and dynamic structural disorder, and computed structures provide insight into the interlayer fluid structures. For the computed systems here, the atomic density profiles (ADPs) normal to the clay basal surface show that the average positions of the different species vary somewhat with the cation. For the monolayer structures here, the ADPs of C_{CO2}, O_{CO2}, and the cation are all centered at the middle of the interlayer at ~2.8 Å to ~3.0 Å from both basal surfaces and become narrower with increasing cation size in each series (Figures 5a-5i). The ADPs of Li^+, Na^+ and Mg^{2+} are significantly broader than those of the other cations, reflecting their relatively small size and ability to move perpendicular to the basal surfaces. The ADPs of the intercalated CO_2 molecules do not vary significantly with cation size, and both O_{CO2} and C_{CO2} share the same plane as the cations, centered at ~2.9 Å from the two basal surfaces. With the alkali cations, the O_{CO2} and C_{CO2} intensities decrease with increasing cation size due to the decreasing amount of intercalated CO_2 (Figures 5a-5e). They do not vary with the different alkaline earth cations, reflecting the independence of the amount of intercalated CO_2 on the cation for this series. This result is consistent with much of the CO_2 being located in free volume in the interlayer rather than being coordinated to the cations, as the energetic results above suggest (Figures 5f-5i).

The average orientation of the O-C-O axis of the intercalated CO_2 molecules lies parallel to the basal surfaces with all the cations (Figures 6a and 6b), as expected from the ADPs of O_{CO2} and C_{CO2} and in agreement with the ^{13}C NMR results above. However, the range of angles probed by the O-C-O vector is somewhat larger with the alkali cations (45º-135º) than with the alkaline earth cations (55º-125º), indicating slightly more dynamically restricted local structural environment with the alkaline earth cations. This difference is probably due to the larger interlayer CO_2 contents with the alkaline earth cations leading to less interlayer space. Visual analysis of the trajectories shows that the individual CO_2 molecules spend part of the

time oriented parallel to the clay layers and part of the time wobbling. The fraction of the time spent wobbling decreases with increasing cation size with the alkali cations but does not change significantly with the alkaline earth cations.

As expected, the computed mean interatomic distance between the cations and CO_2 molecules increases with increasing cation size in the order $Cs^+ > Ba^{2+} > Na^+ > Mg^{2+}$ (Figures 7a -7d). Similarly, cations with small ionic radii are coordinated to the basal hectorite surface at shorter interatomic M-O_b distances (<2.5 Å for Na^+ and Mg^{2+}) than Cs^+ (~3.0 Å). The mean interatomic distances between CO_2 molecules and surface oxygen atoms (O_b), however, do not change with changing cation size. Paralleling the cation-oxygen interatomic distances, the running coordination numbers (RCN) between all the interlayer species vary considerably with the size of the cation. For the monolayer structures, the total coordination of CO_2 molecules by cations, surface O_b atoms, and other CO_2 molecules is ~15.2 for Na^+, Cs^+, and Mg^{2+} but is ~17.0 for Ba^{2+} ions. The RCN of cations with O_b atoms, however, increases from ~2 for Na^+ and Mg^{2+} to ~6.5 and ~7.5 for Ba^{2+} and Cs^+, respectively. The adsorption structure and RCN values for Na- and Cs-hectorites are in excellent agreement with previous studies on hectorites under ambient and elevated *T* and *P* conditions.[14,17,47]

The two-dimensional density maps (also called planar atomic density distributions, or PADDs) for the monolayer structures show that the differences in the RCNs for different cations are the result of significantly different local adsorption environments (Figures 8a-8d). The Na^+ and Mg^{2+} ions are located predominately between two O_b atoms, one on each basal surface giving rise to the O_b RCN of ~2. For Na-hectorite (Figure 8a), the sets of three neighboring site maxima represent the same Na^+ ion (blue) that is hopping between different sites, illustrating a potential pathway for Na^+ diffusion along these narrow channels unhindered by intercalated CO_2. Likewise, the pairs of maxima for Mg^{2+} (Figure 8b) represent the same ion, but in this case the site hopping is more hindered by the increased number of intercalated

CO_2 molecules. As a result, the arrangement of CO_2 molecules is more ordered in Mg-hectorite than in Na-hectorite, where the CO_2 molecules adsorb in narrow channels formed by Na^+ ions and wobble between adjacent hectorite surfaces. This difference correlates well with the more restricted orientation distribution for CO_2 molecules with Mg^{2+} than with Na^+. Nonetheless, there are on average four CO_2 molecules around both Na^+ and Mg^{2+}, consistent with the RCN values (Figures 7a and 7b). For both Na- and Mg-hectorite, the intercalated CO_2 molecules form small clusters, with their arrangement predominantly in a slipped parallel geometry. A small fraction of CO_2 molecules in these clusters are in a distorted T-shaped arrangement, particularly in Mg-hectorite because of its larger number of intercalated CO_2 molecules. A T-shaped arrangement is highly unlikely for Na-hectorite because of the narrow channels formed by the Na^+ ions and CO_2 molecules. For both Na- and Mg-hectorite here, the intercalated CO_2 molecules are adsorbed with one O_{CO2} located near the center of a ditrigonal cavity with the other above a neighboring Si tetrahedron.

Surprisingly, the adsorption structures of CO_2 molecules in Cs- and Ba-hectorite are generally similar to that in Na- and Mg-hectorite, despite the considerably different ionic sizes and interlayer CO_2 contents. Importantly, the RCNs of intercalated CO_2 with surface O_b atoms is ~7-8 with all cations because of the similar adsorption structures described above. The RCN of CO_2 molecules with interlayer cations is ~4 for Na^+-, Cs^+- and Mg^{2+}- and is ~5 with $Ba^{2+,}$ in agreement with the PADDs in Figures 8a-8d. Similarly, the RCN between intercalated CO_2 molecules varies significantly between the structures with alkali cations (~3.5-4) and alkaline earth cations (~5-6) and is due to higher interlayer CO_2 content in the latter case. The contour patterns for CO_2 molecules in Cs-hectorite are more disordered than in the other models due to the lower CO_2/cation ratio and subsequently larger free interlayer space available for librational/wobbling motion. The coordination environments of the Cs^+ and Ba^{2+} ions, however, are quite different (Figures 8c and 8d). The large RCN of Cs^+ with O_b atoms (~7.5)

is due to the fact that on average the Cs^+ ions are located above the center of a ditrigonal cavity of one surface and above a Si tetrahedron on the opposite surface. The Cs^+ ions oscillate between the centers of different ditrigonal cavities and above different Si tetrahedra the, resulting in the disordered contours in Figure 8c. In contrast, the Ba^{2+} ions are adsorbed between Si tetrahedra from both basal surfaces, leading to the average RCN value of ~6.0.

The computed CO_2 orientations and locations in the PADDS are in excellent agreement with the ^{13}C NMR results for Cs-hectorite, which show a restricted environment for the CO_2 molecules in which the time averaged O-C-O vector is parallel to the basal surfaces and the molecules undergo rapid rotation or libration (frequencies > ~10^5 Hz) about an axis perpendicular to their O-C-O axies. The PADD results show that on the 10 ns time scale of the simulations the motion is best thought of as hindered libration rather than free rotation. The tight contours in the PADDs show that the positions of the O_{CO2} are typically quite restricted, even with Cs^+. On the ~ms time scale of probed by the ^{13}C NMR line shapes, however, this may not be true. As shown in our previous experimental study of variably humidified CO_2/hectorite interactions,[9] the absence of CO_2 molecules with O-C-O vectors near 0º and 180º (Figure 6a and 6b) shows that they never experience isotropic reorientation because they are never oriented perpendicular to the basal surfaces.

Residence times

The dynamic interaction among the interlayer species and O_b atoms of the basal surfaces can be quantitatively characterized by the computed mean residence times, which for our systems decrease with increasing cation size for all interatomic pairs (Table 1). Overall, the mean residence times are at least twice as long with smaller cations (Li^+, Na^+, Mg^{2+}, Ca^{2+}) than with larger cations (K^+, Rb^+, Cs^+ and Ba^{2+}). This relationship holds for both the intermittent residence times, $c(t)$, which allow for the possibility that individual atomic pairs

can re-coordinate after becoming separated during the simulation, and the continuous residence times, $C(t)$, which do not allow such re-coordination.[33,35,48] Here, the intermittent residence times are typically about an order of magnitude longer than the continuous ones, as also reported in our previous studies of hydrated interlayers and hectorite exposed to H_2O saturated $scCO_2$.[33,35,48] The $c(t)$ and $C(t)$ values for cation-O_b pairs are consistently longer than those for cation-O_{CO2} and O_b-O_{CO2} coordination, indicating that interactions between cations and basal surfaces are the principal controls of the interlayer structure and dynamics. This conclusion is consistent with the energetic results above, which show that the extent of CO_2 intercalation is strongly dependent on cation-clay interactions (Figures 4a-4f). As the size of interlayer cations increases, the residence times for cation-O_b pairs decreases by an order of magnitude paralleling the expected stronger coordination of smaller cations with clay surfaces, which are dominated by electrostatic interactions. This result is in good agreement with the atomic density maps for especially the alkali cations, which show much more ordered contours for Na^+ than for Cs^+ (Figures 8a and 8c). This difference is less pronounced with the divalent cations, because their higher charge leads to overall stronger coordination with the surface. The cation-O_b residence times are in reasonable agreement with previous simulation studies of hectorite under ambient conditions.[33,35] The cation-CO_2 residence times are longer than O_b-CO_2 residence times, particularly for smaller ions, consistent with their CO_2 solvation energies.[51,68] The difference in cation-CO_2 and O_b-CO_2 residence times decreases with increasing cation size, especially with the alkali cations.

Comparison of Na- and Cs-hectorite

The effects of the exchangeable cations on the structure and energetics of CO_2 molecules intercalated in smectites and the connections to the experimental results are well illustrated by comparing the specific details of the Na- and Cs-hectorite systems. The collapsed interlayer distances for Na- (9.5 Å) and Cs-hectorite (10.7 Å) computed from our simulations

are in good agreement with the values obtained in XRD measurements under vacuum conditions (9.8 Å and Cs-11.08 Å, respectively) and also in good agreement with published computed values, which vary slightly depending on the interatomic potentials used in the simulations.[12,14,16,17,20,69,70,71]

Upon exposure to dry $scCO_2$ at 323 K and 90 bar, the XRD data indicate interlayer expansion for Cs-hectorite but not for Na-hectorite. This is in excellent agreement with our simulations that show that the collapsed structure is the most energetically favorable state for Na-hectorite (Figure 3c). In contrast, there is no energy barrier for Cs-hectorite, and this system favors interlayer expansion when in contact with dry $scCO_2$. Our simulations also indicate that despite the stronger interaction energy between Na^+ and CO_2 molecules (-95 kJ/mol) than between Cs^+ and CO_2 molecules (-30 kJ/mol), CO_2 intercalates in Cs-hectorite because the stronger cation-clay interactions with Na^+ result in a much larger energy cost for expansion from the collapsed to the monolayer structure (~400 kJ/mol) than with Cs^+ (~190 kJ/mol). Thus, the energy difference for the cation-clay interactions between the collapsed state and the basal spacing at which CO_2 intercalation starts is ~175 kJ/mol with Na^+ and only ~35 kJ/mol with Cs^+ (see Figure 4a). Because of the small energy barrier, CO_2 intercalation is favourable in Cs-hectorite, and not in Na-hectorite. These results indicate that the cation-clay interactions play a critical role during CO_2 intercalation.

Conclusions

The intercalation of CO_2 in the interlayers of the smectite clay hectorite with a range of mono- and divalent cations in contact with dry $scCO_2$ at 323 K and 90 bar was quantitatively analyzed by GCMD simulations and *in situ* XRD and NMR experiments. The GCMD results show that clays containing small charge compensating cations, do not spontaneously incorporate CO_2 in their interlayers when exposed to dry $scCO_2$, but that those with larger exchangeable cations do. The thermodynamic energy barriers between the collapsed state of

the clay structure and the onset of CO_2 intercalation are large with small cations and decrease with increasing cation size. With Li^+, Na^+, Mg^{2+}, and Ca^{2+}, the fully collapsed state has the global energy minimum, but with K^+, Rb^+, Cs^+, Sr^{2+}, and Ba^{2+} the monolayer state has the global energy minimum, suggesting that hectorite with these cations should spontaneously intercalate CO_2 and expand but that with the smaller cations it should not. This conclusion is in good agreement with the experimental observation that Na-hectorite does not incorporate CO_2 under these conditions but that Cs-hectorite does. These results are also in good agreement with experimental and GCMD results showing that the similar smectite mineral montmorillonite incorporates dry CO_2 and expands with interlayer NH_4^+ and Cs^+, but not with Na^+. A detailed quantitative analysis of different contributions to the total interaction energies in the investigated systems demonstrates that the structural and energetic characteristics of interlayer expansion with dry $scCO_2$ are largely controlled by the strength of the interactions between the cations and the clay T-O-T structure. This is unlike the case of H_2O intercalation, where the hydration energy of cations dominates the interlayer expansion.[33,35]

Structurally, irrespective of the cation size, charge and CO_2 solvation energy, at monolayer basal spacings the computed average positions of the intercalated CO_2 molecules and the cations are all at the mid-plane of the interlayer. Both the ^{13}C NMR spectra and GCMD simulations show that the intercalated CO_2 molecules are oriented on average with their O-C-O axies parallel to the basal hectorite surfaces. These NMR results for Cs-hectorite show restricted dynamics for the interlayer CO_2 in which they undergo rapid (frequency > $\sim 10^5$ Hz) rotation or libration around an axis perpendicular to their long molecular axies. The GCMD calculations suggest that on the time scale of our simulations (~ 10 ns) this is principally librational hopping among reasonably well-defined sites. The GCMD results suggest that aggregation of the interlayer CO_2 molecules results in both slipped parallel and T-shaped arrangements with slipped parallel dominant. The number of intercalated CO_2 molecules is

larger for interlayers with higher charge cations due to the larger free interlayer space available for CO_2 intercalation due to the smaller number of charge compensating interlayer cations present. Since the cation-clay interactions dominate the thermodynamics of interlayer expansion with dry CO_2, the expansion behavior of smectites with different layer charges or positions of isomorphic substitution (e.g., tetrahedral Al for Si substitution vs. dominantly the octahedral substitution in hectorite and montmorillonite) could be quite different than that discussed here.

Acknowledgements

All the calculations in this work were performed using computational resources at the National Energy Research Scientific Computing Center, which is supported by the Office of Science of the U.S. Department of Energy under ECARP No. m1649. The authors acknowledge iCER computational facility at Michigan State University for additional computational resources. The work was supported by the United States Department of Energy, Office of Science, Office of Basic Energy Sciences, Chemical Sciences, Biosciences, and Geosciences Division through the sister grants DE-FG02-10ER16128 (Bowers, P.I.) and DE-FG02-08ER15929 (Kirkpatrick, P.I.), as well as through its Geosciences program at Pacific Northwest National Laboratory (J.S.L.). H.T.S. was supported by the DOE Office of Fossil Energy at PNNL through the National Energy Technology Laboratory, Morgantown, West Virginia. A.G.K. acknowledges the support of the industrial chair "Storage and Disposal of Radioactive Waste" at the IMT-Atlantique, funded by ANDRA, Areva, and EDF, and of the European Union's Horizon 2020 research and innovation program under grant agreement No. 640979.

Notes

The authors declare no competing financial interest.

Cation	Cation-O_b	Cation-O_{CO2}	O_b-O_{CO2}
	$c(t)$: $C(t)$		
Li^+	10.4 : 0.81	6.3 : 0.65	3.1 : 0.29
Na^+	7.7 : 0.54	3.8 : 0.42	2.4 : 0.21
K^+	2.1 : 0.31	1.9 : 0.29	1.1 : 0.13
Rb^+	0.9 : 0.14	1.1 : 0.09	0.9 : 0.08
Cs^+	0.7 : 0.08	0.8 : 0.02	0.8 : 0.05
Mg^{2+}	12.1 : 1.0	8.4 : 0.64	5.5 : 0.31
Ca^{2+}	8.8 : 0.79	6.2 : 0.48	3.8 : 0.24
Sr^{2+}	5.2 : 0.51	4.1 : 0.34	2.1 : 0.15
Ba^{2+}	3.1 : 0.35	2.5 : 0.25	1.3 : 0.12

Table 1. Calculated intermittent $c(t)$ and continuous $C(t)$ residence times (ns) for different atomic pairs for monolayer basal spacing (12.4 Å) in the interlayers of hectorite with different charge compensating cations at 323 K and 90 bar.

FIGURES

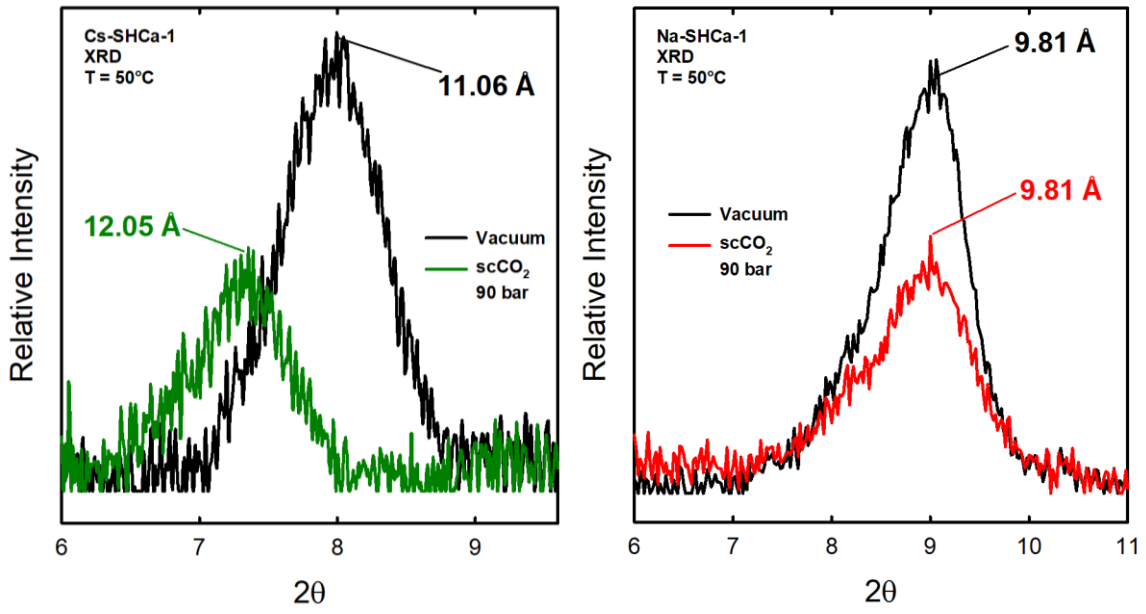

Figure 1. X-ray diffraction tracings of the Cs-SHCa-1 (left) and the Na-SHCa-1 (right) clay under vacuum (10^{-3} Torr, 323 K) and during exposure to 90 bar $scCO_2$ at 323 K. Note that the smaller peak intensities in the samples exposed to $scCO_2$ are due to signal attenuation by the dense CO_2 fluid.

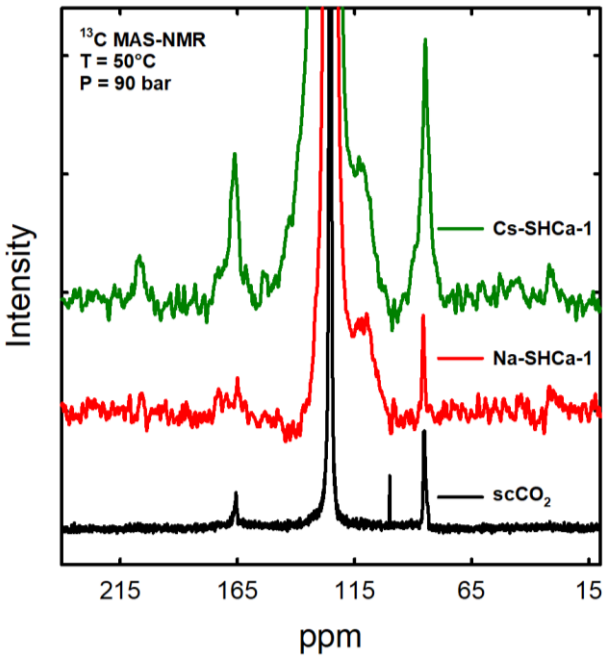

Figure 2. ^{13}C MAS NMR spectra Cs-SHCa-1 in $scCO_2$ (top), Na-SHCa-1 in $scCO_2$ (middle), and a rotor only filled with $scCO_2$, all at 90 bar pressure and 323 K. The broad peak near 110 ppm is the ^{13}C background of the NMR probe, and the narrow singularity near 100 ppm reflects a DC offset in the receiver channels.

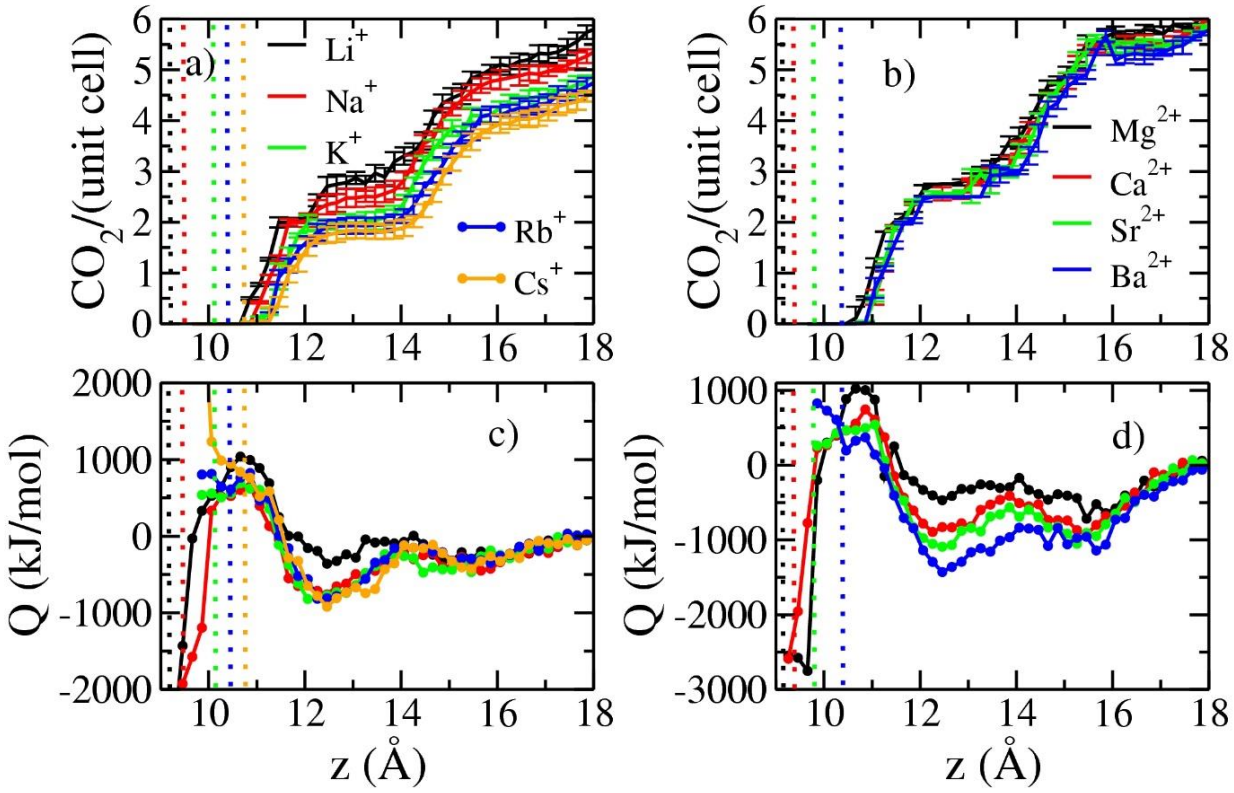

Figure 3. a) and b) are the average number of intercalated CO_2 molecules (per unit cell); c) and d) are the computed immersion energies for hectorite models with different charge compensating cations as functions of interlayer basal spacing at 323 K and 90 bar. Dotted vertical lines indicate the collapsed interlayer distances for every cations used in our study. The reference state for computing the immersion energies is the 18.0 Å basal spacing.

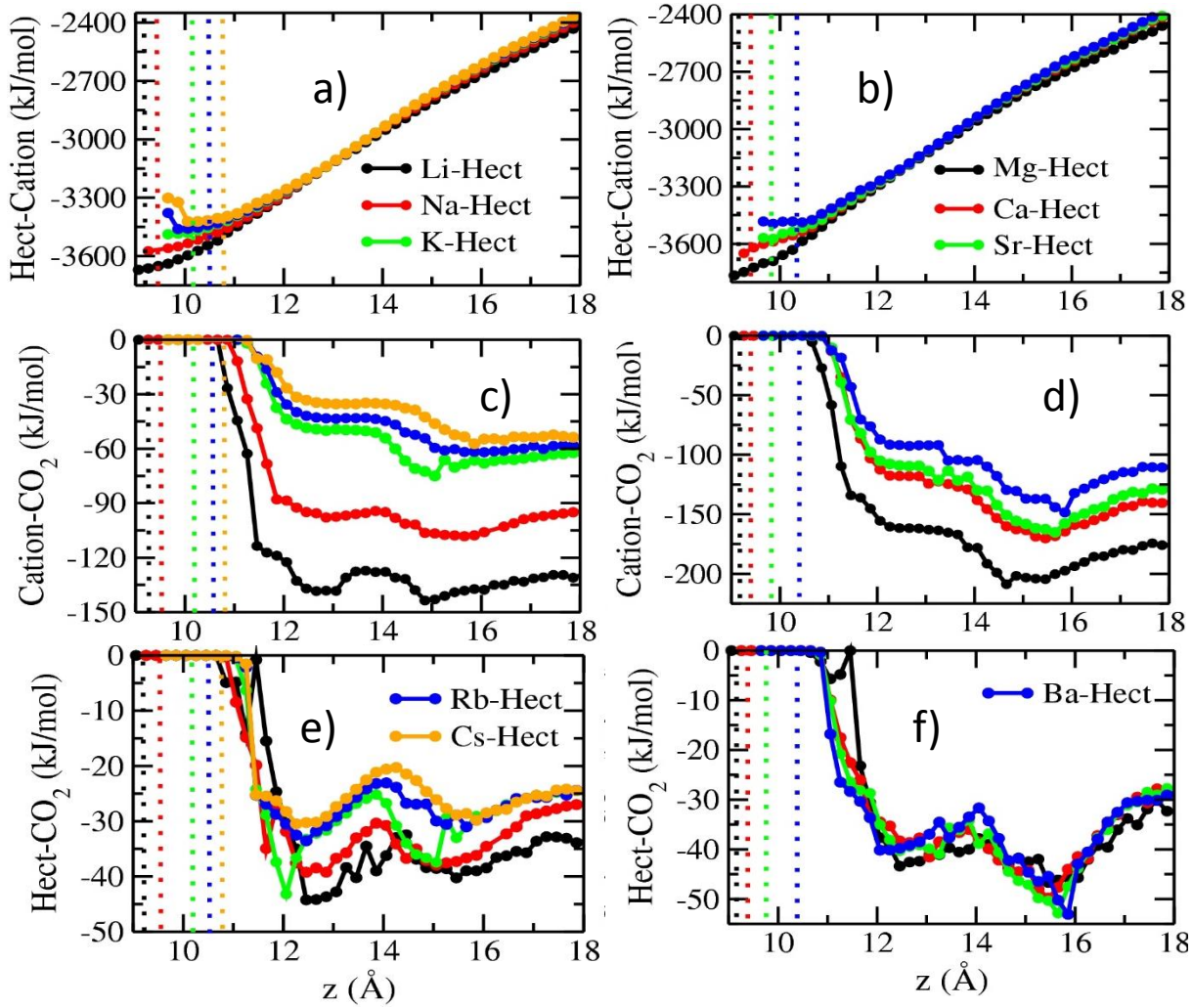

Figure 4. Computed variation in interaction energies between 3 different pairs (a) and b) are Hectorite–Cation (top), c) and d) are Cation–CO_2 (middle), e) and f) are Hectorite-CO_2 (bottom)) as functions of interlayer spacing using hectorite with different of mono- and di-valent cations at 323 K and 90 bar. Dotted vertical lines indicate the collapsed interlayer distances for every cations used in our study.

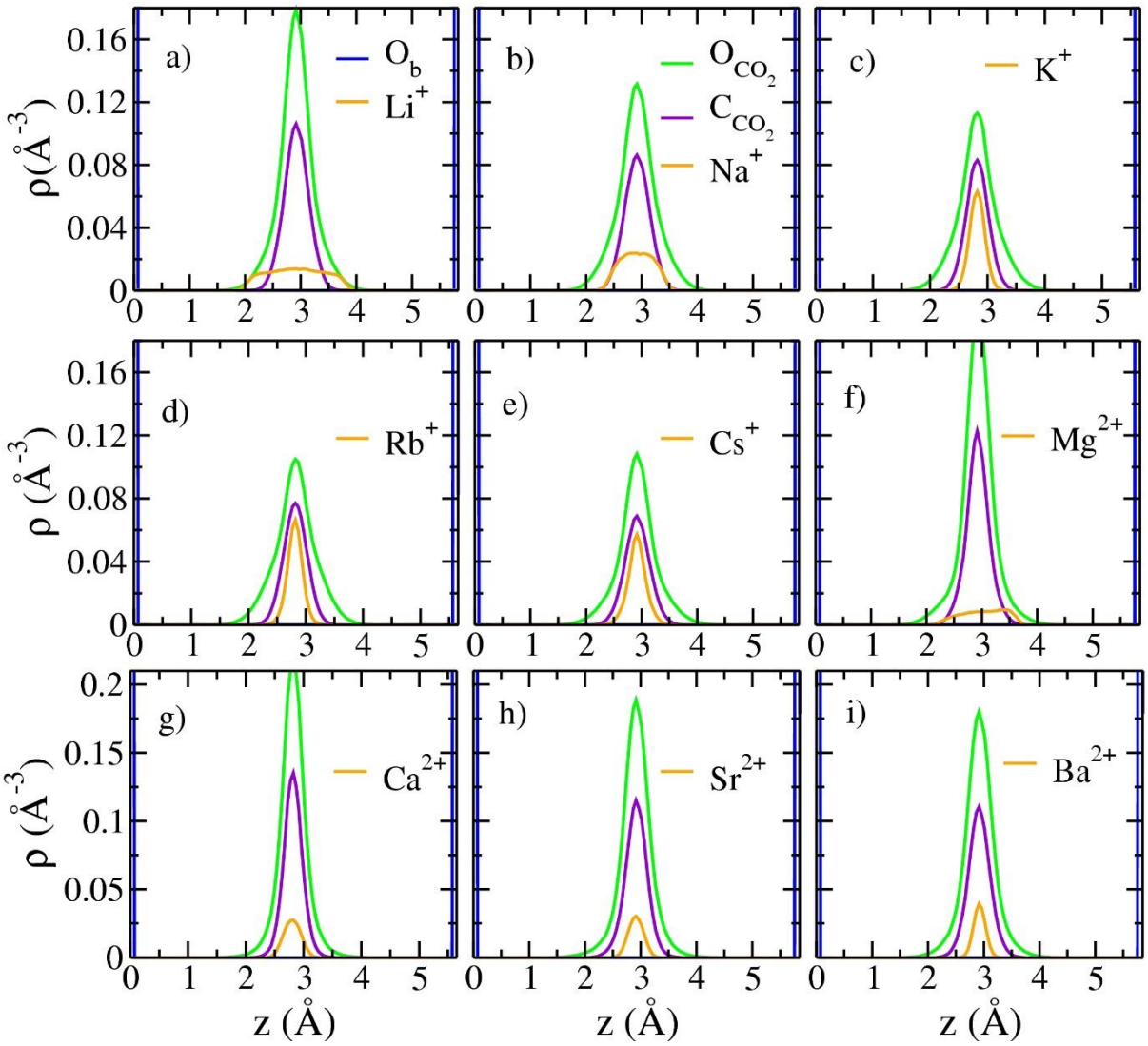

Figure 5. Computed atomic density profiles of O_b (dark blue vertical lines), interlayer mono- and divalent cations (orange), O_{CO2} (green) and C_{CO2} (violet) of hectorite as functions of distance from the basal clay surface at monolayer distances (12.4 Å) under conditions of 323 K and 90 bar.

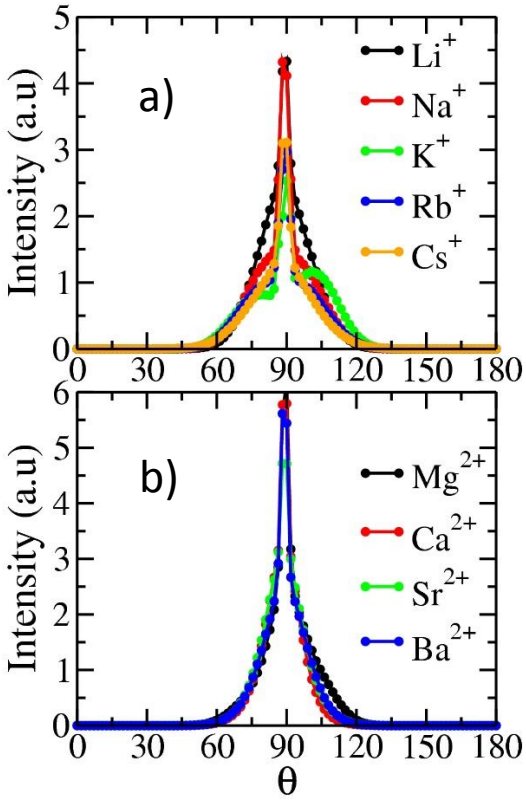

Figure 6. Computed orientational distributions of intercalated CO_2 molecules in the interlayers of hectorite at monolayer distances under 323 K and 90 bar conditions with different charge compensating cations. Θ is the angle between the O-O vector of a CO_2 molecule and the normal to the hectorite basal surface. a) monovalent cations. b) divalent cations.

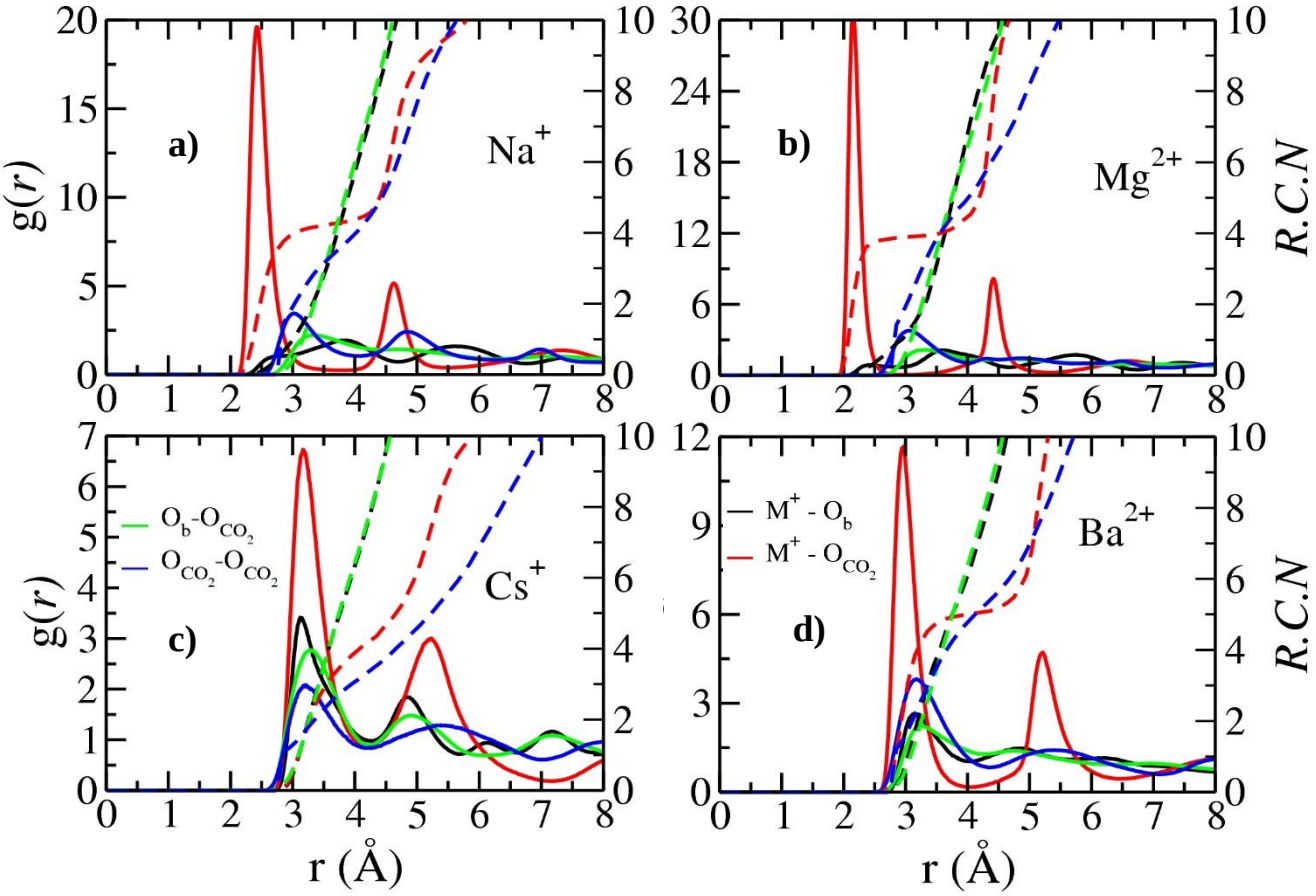

Figure 7. Radial distribution functions (RDFs, solid lines) and corresponding running coordination numbers (RCNs, dashed lines) for different atomic pairs in the interlayers of a) Na- b) Mg- c) Cs- d) Ba-hectorite at monolayer distances under 323 K and 90 bar conditions.

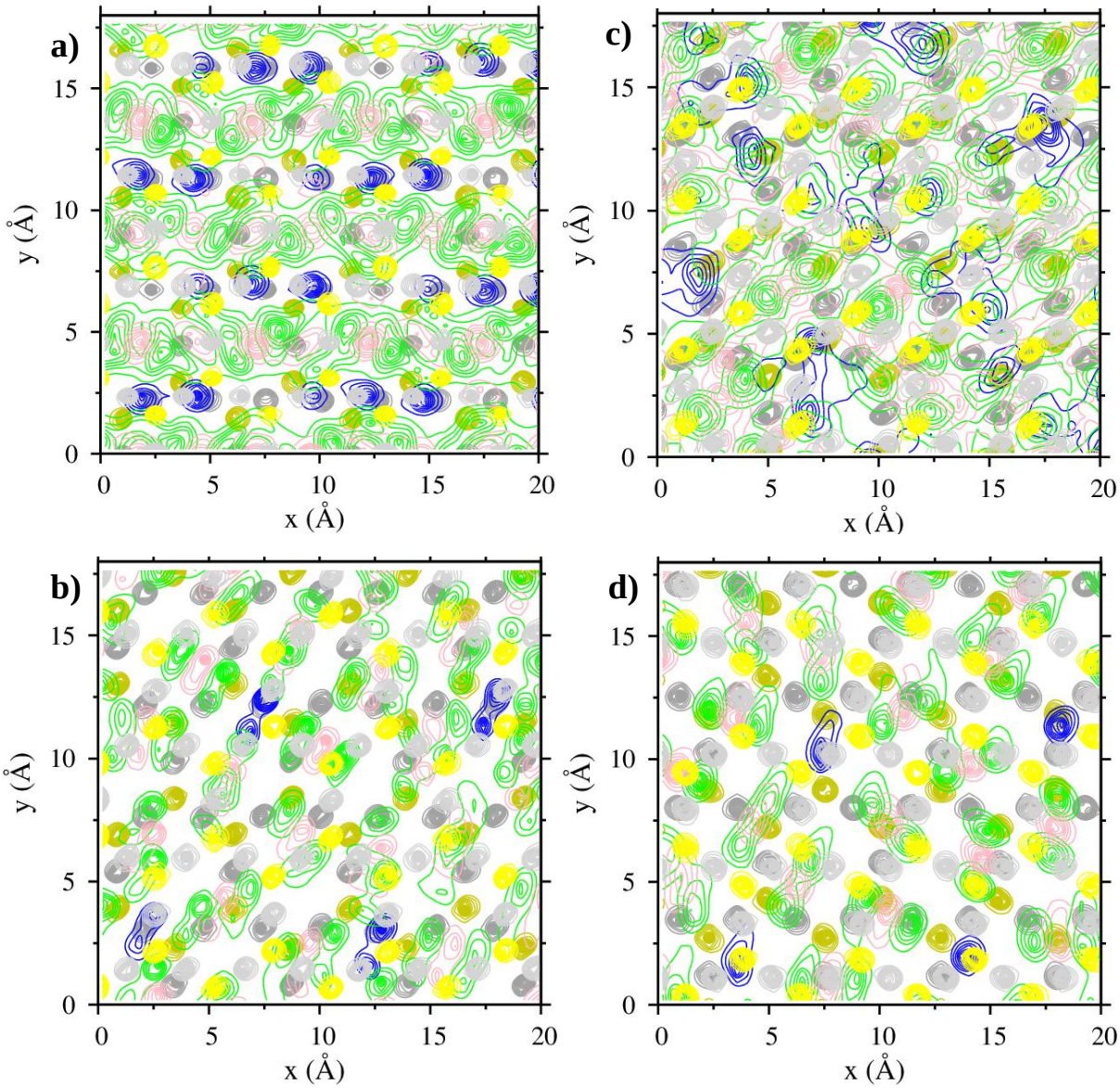

Figure 8. Computed PADDs of interlayer metal cations and intercalated CO_2 molecules in hectorite interlayers at monolayer distances and 323 K and 90 bar. a) Na^+ and CO_2 in Na-hectorite; b) Mg^{2+} and CO_2 in Mg-hectorite; c) Cs^+ and CO_2 in Cs-hectorite; d) Ba^{2+} and CO_2 in Ba-hectorite. Color code: O_b – gray (dark and light), Si – yellow (dark and light), Cation (Na^+, Cs^+, Mg^{2+}, Ba^{2+}) – blue, O_{CO2} – green, C_{CO2} – pink, Dark colors correspond to the O_b and Si of one hectorite basal surface, and light colors correspond to those atoms of the opposite basal surface.

References

1. Gauss, I. Role and Impact of CO_2-Rock Interactions During CO_2 Storage in Sedimentary Rocks. *Int. J. Green. Gas Cont.* **2010,** *4*, 73-89.
2. Lackner, K. S. A Guide to CO_2 Sequestration. *Science* **2003,** *300*, 1677-1678.
3. Benson, S. M.; Cole, D. R. CO_2 Sequestration in Deep Sedimentary Formations. *Elements* **2008,** *4*, 325-331.
4. Bachu, S.; Bonijoly, D.; Bradshaw, J.; Burruss, R.; Holloway, S.; Christensen, N. P.; Mathiassen, O. M. CO_2 Storage Capacity Estimation: Methodology and Gaps. *Int. J. Green. Gas Cont.* **2007,** *1*, 430-443.
5. Wilkin, R. T.; Digiulio, D. Geochemical Impacts to Groundwater from Geologic Carbon Sequestration: Controls on pH and Inorganic Carbon Concentrations from Reaction Path and Kinetic Modeling. *Environ. Sci. Technol.* **2010,** *44*, 4821-4827.
6. Berrezueta, E.; Menendez, G.-L.; Breitner, D.; Luquot, L. Pore System Changes During Experimental CO_2 Injection into Detritic Rocks. Studies of Potential Storage Rocks from Some Sedimentary Basins of Spain. *Int. J. Green. Gas Cont.* **2013,** *4*, 73-89
7. Meakin, P.; Tartakovsky, A. M. Modeling and Simulation of Pore-Scale Multiphase Fluid Flow and Reactive Transport in Fractured and Porous Media. *Rev. Geophys.* **2009**, *47*, RG3002.
8. Davis, A. J.; Kent, B. D. Surface Complexation Modeling in Aqueous Geochemistry. *Rev. Mineral.* **1990**, *23*, 177-260.
9. Bowers, G. M.; Schaef, H. T.; Loring, J. S.; Hoyt, D. W.; Burton, S. D.; Walter, E. D.; Kirkpatrick, R. J. Role of Cations in CO_2 Adsorption, Dynamics and Hydration in Smectite Clays under In Situ Supercritical CO_2 Conditions. *J. Phys. Chem. C* **2017,** *121*, 577-592.
10. Wang, Z.; Felmy, A. R.; Thompson, C. J.; Loring, J. S.; Joly, A. G.; Rosso, K. M.; Schaef, H. T.; Dixon, D. A. Near-Infrared Spectroscopic Investigation of Water in Supercritical CO_2 and the effect of $CaCl_2$. *Fluid Phase Equil.* **2013,** *338*, 155-163.
11. Giesting, P.; Guggenheim, S.; van Groos, A. F. K.; Busch, A. Interaction of Carbon Dioxide with Na-Exchanged Montmorillonite at Pressures to 640 bar: Implications for CO_2 Sequestration. *Int. J. Green. Gas Cont.* **2012,** *8*, 73-81.
12. Giesting, P.; Guggenheim, S.; van Groos, A. F. K.; Busch, A. X-ray Diffraction Study of K- and Ca-Exchanged Montmorillonites in CO_2 Atmospheres. *Environ. Sci. Technol.* **2012,** *46*, 5623-5630.
13. Lee, M.-S.; McGrail, B. P.; Glezakou, V.-A. Microstructural Response of Variably Hydrated Ca-rich Montmorillonite to Supercritical CO_2. *Environ. Sci. Technol.* **2014,** *48*, 8612-8619.
14. Ilton, E. S.; Schaef, H. T.; Qafoku, O.; Rosso, K. M.; Felmy, A. R. In Situ X-ray Diffraction Study of Na^+ Saturated Montmorillonite Exposed to Variably Wet Supercritical CO_2. *Environ. Sci. Technol.* **2012,** *46*, 4241-4248.
15. Guggenheim, S.; van Groos, A. F. K. An Integrated Experimental System for Solid-Gas-Liquid Environmental Cells. *Clays Clay Miner.* **2014,** *62*, 470-476.

16. Rother, G.; Ilton, E. S.; Wallacher, D.; Hauss, T.; Schaef, H. T.; Qafoku, O.; Rosso, K. M.; Felmy, A. R.; Krukowski, E. G.; Stack, A. G. et al. CO_2 Sorption to Subsingle Hydration Layer Montmorillonite Clay Studies by Excess Sorption and Neutron Diffraction Measurements. *Environ. Sci. Technol.* **2013,** *47*, 205-211.

17. Schaef, H. T.; Ilton, E. S.; Qafoku, O.; Martin, P. F.; Felmy, A. R.; Rosso, K. M. In Situ XRD study of Ca^{2+} Saturated Montmorillonite (STx-1) Exposed to Anhydrous and Wet Supercritical Carbon Dioxide. *Int. J. Green. Gas Cont.* **2012,** *6*, 220-229.

18. Romanov, V. N. Evidence of Irreversible CO_2 Intercalation in Montmorillonite. *Int. J. Green. Gas Cont.* **2013,** *14*, 220-226.

19. Schaef, H. T.; Loring, J. S.; Glezakou, V. A.; Miller, Q. R. S.; Chen, J.; Owen, A. T.; Lee, M.-S.; Ilton, E. S.; Felmy, A. R.; McGrail, B. P. et al. Competitive Sorption of CO_2 and H_2O in 2:1 Layer Phyllosilicates. *Geochim. Cosmochim. Acta* **2015,** *161*, 248-257.

20. Loring, J. S.; Schaef, H. T.; Turcu, R. V. F.; Thompson, C. J.; Miller, Q. R.; Martin, P. F.; Hu, J.; Hoyt, D. W.; Qafoku, O.; Ilton, E. S. et al. In Situ Molecular Spectroscopic Evidence for CO_2 Intercalation into Montmorillonite in Supercritical Carbon Dioxide. *Langmuir* **2012,** *28*, 7125-7128.

21. Loring, J. S.; Ilton, E. S.; Chen, J.; Thompson, C. J.; Martin, P. F.; Benezeth, P.; Rosso, K. M.; Felmy, A. R.; Schaef, H. T. In Situ Study of CO_2 and H_2O Partitioning Between Na-Montmorillonite and Variably Wet Supercritical Carbon Dioxide. *Langmuir* **2014,** *30*, 6120-6128.

22. Loring, J. S.; Schaef, H. T.; Thompson, C. J.; Turcu, R. V. F.; Miller, Q. R.; Chen, J.; Hu, J.; Hoyt, D. W.; Martin, P. F.; Ilton, E. S. et al. Clay Hydration/Dehydration in Dry to Water-Saturated Supercritical CO_2: Implications for Caprock Integrity. *Energy Procedia* **2013,** *37*, 5443-5448.

23. Krukowski, E. G.; Goodman, A.; Rother, G.; Ilton, E. S.; Guthrie, G.; Bodnar, R. J. FT-IR Study of CO_2 Interaction with Na^+ Exchanged Montmorillonite. *Appl. Clay Sci.* **2015,** *114*, 61-68.

24. Bowers, G. M.; Hoyt, D. W.; Burton, S. D.; Ferguson, B. O.; Varga, R.; Kirkpatrick, R. J. In Situ ^{13}C and ^{23}Na Magic Angle Spinning NMR Investigation of Supercritical CO_2 Incorporation in Smectite-Natural Organic Matter Composites. *J. Phys. Chem. C* **2014,** *118*, 3564-3573.

25. Bowers, G. M.; Bish, D. L.; Kirkpatrick, R. J. Cation Exchange at the Mineral-Water Interface: H_3O^+/K^+ Competition at the Surface of Nano-Muscovite. *Langmuir* **2008**, *24*, 10240-10244.

26. Bowers, G. M.; Singer, J. W.; Bish, D. L.; Kirkpatrick, R. J. Alkali Metal and H_2O Dynamics at the Clay/Water Interface. *J. Phys. Chem. C* **2011**, *115*, 23395-23407.

27. Marry, V.; Dubois, E.; Malikova, N.; Durand-Vidal, S.; Longeville, S.; Breu, J. Water Dynamics in Hectorite Clays: Influence of Temperature Studied by Coupling Neutron Spin Echo and Molecular Dynamics. *Environ. Sci. Technol.* **2011**, *45*, 2850-2855.

28. Weiss, C. A.; Kirkpatrick, R. J.; Altaner, S. P. Variations in Interlayer Cation Sites of Clay Minerals as Studied by ^{133}Cs MAS Nuclear Magnetic Resonance Spectroscopy. *Amer. Mineral.* **1990**, *75*, 970-982.

29. Weiss, C. A.; Kirkpatrick, R. J.; Altaner, S. P. The Structural Environments of Cations Adsorbed onto Clays – ^{133}Cs Variable-Temperature MAS NMR Spectroscopic Study of Hectorite. *Geochim. Cosmochim. Acta* **1990**, *54*, 1655-1669.

30. Morrow, C. P.; Yazaydin, A. O.; Krishnan, M.; Bowers, G. M.; Kalinichev, A. G.; Kirkpatrick. R. J. Structure, Energetics and Dynamics of Smectite Clay Interlayer Hydration: Molecular Dynamics and Metadynamics Investigation of Na-Hectorite. *J. Phys. Chem. C* **2013**, *117*, 5172-5187.

31. Reddy, U. V.; Bowers, G. M.; Loganathan, N.; Bowden, M.; Yazaydin, A. O.; Kirkpatrick, R. J. Water Structure and Dynamics in Smectites: ^{2}H NMR Spectroscopy of Mg, Ca, Sr, Cs and Pb-Hectorite. *J. Phys. Chem. C* **2016,** *120*, 8863-8876.

32. Marry, V.; Malikova, N.; Cadene, A.; Dubois, E.; Durand-Vidal, S.; Turq, P.; Breu, J.; Longeville, S.; Zanotti, J. M. Water Diffusion in a Synthetic Hectorite by Neutron Scattering – Beyond the Isotropic Translational Model. *J. Phys.: Cond. Matter* **2008**, *20*, 104205.

33. Loganathan, N.; Yazaydin, A. O.; Bowers, G. M.; Kalinichev, A. G.; Kirkpatrick, R. J. Structure, Energetics and Dynamics of Cs^{+} and H_2O in Hectorite: Molecular Dynamics Simulations with Unconstrained Substrate Surface. *J. Phys. Chem. C* **2016**, *120*, 10298-10310.

34. Porion, P.; Faugere, A. M.; Delville, A. Multiscale Water Dynamics within Dense Clay Sediments Probed by ^{2}H Multiquantum NMR Relaxometry and Two-Time Stimulated Echo NMR Spectroscopy. *J. Phys. Chem. C* **2013**, *117*, 26119-26134.

35. Loganathan, N.; Yazaydin, A. O.; Bowers, G. M.; Kalinichev, A. G.; Kirkpatrick, R. J. Cation and Water Structure, Dynamics and Energetics in Smectite Clays: A Molecular Dynamics Study of Ca-Hectorite. *J. Phys. Chem. C* **2016**, *120*, 12429-12439.

36. Greathouse, J. A.; Hart, D. B.; Bowers, G. M.; Kirkpatrick, R. J.; Cygan, R. T. Molecular Simulation of Structure and Diffusion at Smectite-Water Interfaces: Using Expanded Clay Interlayers as Model Nanopores. *J. Phys. Chem. C* **2015**, *119*, 17126-17136.

37. Ngouana-Wakou. B. F.; Kalinichev, A. G. Structural Arrangements of Isomorphic Substitutions in Smectites: Molecular Simulation of the Swelling Properties, Interlayer Structure and Dynamics of Hydrated Cs-Montmorillonite Revisited with New Clay Models. *J. Phys. Chem. C* **2014**, *118*, 12758-12773.

38. Sato, T.; Watanabe, T.; Otuka, R. Effects of Layer Charge, Charge Location, and Energy Change on Expansion Properties of Dioctahedral Smectites. *Clays Clay Miner.* **1992**, *29*, 873-882.

39. Wang, J.; Kalinichev, A. G.; Kirkpatrick, R. J. Effects of Substrate Structure and Composition on the Structure, Dynamics and Energetics of Water at Mineral Surfaces: A Molecular Dynamics Modeling Study. *Geochim. Cosmochim. Acta* **2006,** *70*, 562-582.

40. Botan, A.; Rotenberg, R.; Marry, V.; Turq, P.; Noetinger, B. Carbon Dioxide in Montmorillonite Clay Hydrates: Thermodynamics, Structure and Transport from Molecular Simulation. *J. Phys. Chem. C* **2010**, *114*, 14962-14969.

41. Kadoura, A.; Nair, A. K. N.; Sun, S. Molecular Simulation Study of Montmorillonite in Contact with Variably Wet Supercritical Carbon Dioxide. *J. Phys. Chem. C* **2017**, *121*, 6199-6208.

42. Myshakin, E. M.; Saidi, W. A.; Romanov, V. N.; Cygan, R. T.; Jordan, K. D. Molecular Dynamics Simulations of Carbon Dioxide Intercalation in Hydrated Na-Montmorillonite. *J. Phys. Chem. C* **2013**, *117*, 11028-11039.

43. Makaremi, M.; Jordan, K. D.; Guthrie, G. D.; Myshakin, E. M. Multiphase Monte Carlo and Molecular Dynamics Simulations of Water and CO_2 Intercalation in Montmorillonite and Beidellite. *J. Phys. Chem. C* **2015**, *119*, 15112-15124.

44. Rao, A.; Leng, Y. Molecular Understanding of CO_2 and H_2O in a Montmorillonite Clay Interlayer Under CO_2 Geological Sequestration Conditions. *J. Phys. Chem. C* **2016**, *120*, 2642-2654.

45. Rao, A.; Leng, Y. Effect of Layer Charge on CO_2 and H_2O Intercalations in Swelling Clays. *Langmuir* **2016**, *32*, 11366-11374.

46. Sena, M. M.; Morrow, C. P.; Kirkpatrick, R. J.; Krishnan, M. Structure, Energetics, and Dynamics of Supercritical Carbon Dioxide at Smectite Mineral-Water Interfaces: Molecular Dynamics Modeling and Adaptive Force Investigation of CO_2/H_2O Mixtures Confined in Na-Montmorillonite. *Chem. Mater.* **2015**, *27*, 6946-6959.

47. Yazaydin, A. O.; Bowers, G. M.; Kirkpatrick, R. J. Molecular Dynamics Modeling of Carbon Dioxide, Water and Natural Organic Matter in Na-Hectorite. *Phys. Chem. Chem. Phys.* **2015**, *17*, 23356-23367.

48. Loganathan, N.; Yazaydin, A. O.; Bowers, G. M.; Kalinichev, A. G.; Kirkpatrick, R. J. Molecular Dynamics Study of CO_2 and H_2O Intercalation in Smectite Clays: Effect of Temperature and Pressure on Interlayer Structure and Dynamics in Hectorite. *J. Phys. Chem. C* **2017**, *121*, 24527-24540.

49. Luquot, L.; Gouze, P. Experimental Determination of Porosity and Permeability Changes Induced Injection of CO_2 into Carbonate Rocks. *Chem. Geol.* **2009**, *265*, 148-159.

50. Vickerd, M. A.; Thring, R. W.; Arocena, J. M.; Li, J. B. Changes in Porosity due to Acid Gas Injection as Determined by X-ray Computed Tomography. *J. Can. Petrol. Techn.* **2006**, *45(8)*, 17-22.

51. Schaef, H. T.; Loganathan, N.; Bowers, G. M.; Kirkpatrick, R. J.; Yazaydin, A. O.; Burton, S. D.; Hoyt, D. W.; Ilton, E. S.; Thanthiriwatte, K. S.; Dixon, D. A. et al. Tipping Point for Expansion of Layered Aluminosilicates in Weakly Polar Solvents: Supercritical CO_2. *Appl. Mater. Interf.* **2017**, *9*, 36783-36791.

52. Bowers, G. M.; Singer, J. W.; Bish, D. L.; Kirkpatrick, R. J. Structure and Dynamical Relationships of Ca^{2+} and H_2O in Smectite/^2H_2O Systems. *Amer. Mineral*. **2014**, *99*, 318-331.

53. Hoyt, D. W.; Turcu, R. V. F.; Sears, J. A.; Rosso, K. M.; Burton, S. D.; Felmy, A.; Hu, J. Z. High-Pressure Magic Angle Spinning Nuclear Magnetic Resonance. *J. Magn. Reson.* **2011**, *212*, 378−385.

54. Turcu, R. V. F.; Hoyt, D. W.; Rosso, K. M.; Sears, J. A.; Loring, J. S.; Felmy, A.; Hu, J. Z. Rotor Design for High Pressure Magic Angle Spinning Nuclear Magnetic Resonance. *J. Magn. Reson.* **2013**, *226*, 64−69.

55. Tenorio, R. P.; Alme, L. R.; Engelsberg, M.; Fossum, J. O.; Hallwass, F. Geometry and Dynamics of Intercalated Water in Na-Fluorohectorite Clay Hydrates. *J. Phys. Chem. C* **2008**, *112*, 575-580.

56. Dazas, B.; Lanson, B.; Breu, J.; Robert, J-L.; Pelletier, M.; Ferrage, E. Smectite Fluorination and its Impact on Interlayer Water Content and Structure: A way to Fine Tune the Hydrophobicity of Clay Surfaces? *Micro. Meso. Mater.* **2013**, *181*, 233-247.

57. Lowenstein, W. The Distribution of Aluminium in the Tetrahedra of Silicates and Aluminates. *Amer. Mineral*. **1954**, *39*, 92-96.

58. Boinepalli, S.; Attard, P. Grand Canonical Molecular Dynamics. *J. Chem. Phys*. **2003**, *119*, 12769-12775.

59. Dubbeldam, D.; Calero, S.; Ellis, D. E.; Snurr, R. Q. RASPA: Molecular Simulation Software for Adsorption and Diffusion in Flexible Nanoporous Materials. *Mol. Sim.* **2016**, *42*, 81-101.

60. Young, D. A.; Smith, D. E. Simulations of Clay Mineral Swelling and Hydration: Dependence upon Interlayer Ion Size and Charge. *J. Phys. Chem. B* **2000**, *104*, 9163-9170.

61. Cygan, R. T.; Liang, J.-J.; Kalinichev, A. G. Molecular Models of Hydroxide, Oxyhydroxide and Clay Phases and the Development of a General Force Field. *J. Phys. Chem. B* **2004,** *108*, 1255-1266.

62. Cygan, R. T.; Romanov, V. N.; Myshakin, E. M. Molecular Simulation of Carbon Dioxide Capture by Montmorillonite Using an Accurate and Flexible Force Field. *J. Phys. Chem. C* **2012,** *116*, 13079-13091.

63. Allen, M. P.; Tildesley, D. J. Computer Simulations of Liquids; Clarendon Press: Oxford, U.K., 1987.

64. Peng, D. Y.; Robinson, D. B. A New Two-Constant Equation of State. *Ind. Eng. Chem. Fundam.* **1976,** *15*, 59-64.

65. Smith, D. E. Molecular Computer Simulations of the Swelling Properties and Interlayer Structure of Cesium Montmorillonite. *Langmuir* **1998**, *14*, 5959-5967.

66. Berend, I.; Cases, J. M.; Francois, M.; Uriot, J. P.; Michot, L.; Masion, A.; Thomas, F., Mechanism of Adsorption and Desorption of Water-Vapor by Homoionic Montmorillonites 2. The Li^+, Na^+, K^+, Rb^+, Cs^+-Exchanged Forms. *Clays Clay Miner.* **1995,** *43*, 324-336.

67. Hemmen, H.; Rolseth, E. G.; Fonseca, D. M.; Hansen, E. L; Fossum, J. O.; Plivelic, R. X-ray Studies of Carbon Dioxide Intercalation in Na-Fluorohectorite Clay at Near-Ambient Conditions. *Langmuir* **2012**, *28*, 1678-1682.

68. Criscenti, L. J.; Cygan, R. T. Molecular Simulations of Carbon Dioxide and Water: Cation Solvation. *Environ. Sci. Technol.* **2013**, *47*, 87-94.

69. Sutton, R.; Sposito, G. Molecular Simulation of Interlayer Structure and Dynamics in 12.4Å Cs-Smectite Hydrates. *J. Coll. Interf. Sci*. **2001**, *237*, 174-184.

70. Seidl, W.; Breu, J. Single Crystal Structure Refinement of Tetramethylammonium-Hectorite. *Z. Kristallogr*. **2005**, *220*, 169-176.

71. Kosakowski, G.; Churakov, S. V.; Thoenen, T. Diffusion of Na and Cs in Montmorillonite. *Clays Clay Miner.* **2008**, *56*, 190-206.

TOC Graphic